

Photoelectron spectroscopy of negatively charged bismuth clusters: Bi_2^- , Bi_3^- , and Bi_4^-

Mark L. Polak, Joe Ho, Gustav Gerber,^{a)} and W. C. Lineberger

Joint Institute for Laboratory Astrophysics, National Institute of Standards and Technology and University of Colorado and Department of Chemistry and Biochemistry, University of Colorado, Boulder, Colorado 80309-0440

(Received 15 April 1991; accepted 21 May 1991)

We have recorded the 351 nm photoelectron spectra of Bi_2^- , Bi_3^- , and Bi_4^- . The spectrum of Bi_2^- shows transitions to at least seven electronic states of Bi_2 neutral, four of which are observed with vibrational resolution. Term energies, bond lengths, and vibrational frequencies are obtained for the anion ground state and for the first three excited states of Bi_2 . These results are compared to previous spectroscopic measurements and to the *ab initio* calculations presented in the accompanying paper. The photoelectron spectrum of Bi_3^- reveals some of the electronic structure of Bi_3 and the results are discussed in comparison to recent theoretical work. Adiabatic electron affinities are obtained for Bi_2 [1.271(8) eV] and for Bi_3 [1.60(3) eV]. The electron affinity of Bi_4 is estimated from the onset of photodetachment to be 1.05(10) eV.

I. INTRODUCTION

Despite great advances in the study of metal clusters in recent years, direct spectroscopic investigation of cluster properties remains difficult experimentally. Because of mass selectivity and high sensitivity, negative ion photoelectron spectroscopy is a particularly useful method for spectroscopic determination of basic properties of neutral and anionic metal clusters, determining molecular parameters such as geometries, electronic structure, vibrational frequencies, and electron affinities. Many of these studies¹⁻³ have focused on transition metal cluster anions, particularly^{2,3} the late d^9 and d^{10} transition metals (the Ni and Cu groups). In this study, the first of a series on main group metal clusters, we investigate three group V metal cluster anions Bi_2^- , Bi_3^- , and Bi_4^- .

Because main group metals play such an important role in semiconductor materials, understanding the electronic structure of the small clusters can be of considerable importance. In contrast to transition metals, where the presence of open ($n-1$) d shells can result in very high densities of low-lying electronic states even for dimers,⁴ bonding in the main group metals (groups III-VI) mainly results from atomic open np shells, generating a rich, but generally discernible spectrum of low-lying electronic states, at least for small clusters ($n \leq 4$). Negative ion photoelectron spectroscopy has been used by other investigators^{5,6} to study main group metal and semiconductor clusters. A primary emphasis of the studies involving main group metals has been the determination of electron affinities for a large range of cluster sizes. In this study of Bi_n^- ($n = 2-4$), relatively high resolution (8-10 meV) permits a comparatively detailed look at the electronic structure and molecular parameters of the anions and corresponding neutrals, particularly for the dimer.

Neutral bismuth clusters have been the subject of considerable previous investigation, particularly the dimer and tetramer. There have been numerous investigations of the electronic spectrum of Bi_2 in both the gas phase⁷⁻¹² and using matrix isolation;¹³⁻¹⁶ some of these studies^{10,11} have partially characterized the low-lying electronic states that are accessed in our photoelectron spectrum (< 2.1 eV above the ground state). In addition, Ehret and Gerber¹⁷ have measured the equilibrium dissociation energy of Bi_2 to be $16\,778(5) \text{ cm}^{-1}$ [2.0802(6) eV] using double resonance polarization spectroscopy. Very recently, Wang *et al.*¹⁸ have measured the He(I) photoelectron spectra of the group V neutral dimers, Bi_2 , Sb_2 , and As_2 , probing the electronic structure of the respective cations.

The gas phase optical spectroscopic studies^{10,11} of Bi_2 which have examined the low-lying electronic states of Bi_2 are of particular interest to the present study. Gerber *et al.*¹⁰ identified two low-lying electronic states labeled B and A' at approximately 5000 and 8000 cm^{-1} above the ground state. These states were thermally populated and observed as lower states of an electronic transition. Resolution of laser-induced fluorescence permitted vibrational parameters to be determined for these states; however, parity selection rules prohibited spectroscopic linkage of these states to the ground state in that experiment. Therefore, term energies could only be estimated through temperature dependence studies of spectral intensities. An advantage of photoelectron spectroscopy is much less restrictive selection rules,¹⁹ which permit these term energies to be determined directly in the present study. Effantin *et al.*¹¹ observed a state labeled B' with a term energy near $10\,800 \text{ cm}^{-1}$ in resolved fluorescence resulting from ultraviolet (3514 and 3618 Å) excitation of ground state Bi_2 . A feature in the Bi_2^- photoelectron spectrum is attributed to the B' state.

In contrast to Bi_2 , very little is known about Bi_3 , as it has not been studied spectroscopically. The cation Bi_3^+ has

^{a)} JILA Visiting Fellow. Permanent Address: Fakultät für Physik, Universität Freiburg, W 7800 Freiburg, Germany.

been detected in many contexts through mass spectrometry.²⁰ However, Kohl *et al.*²¹ have pointed out that detection of Bi_3^+ does not necessarily correlate with the presence of neutral Bi_3 , as the Bi_3^+ cation may be formed from fragmentation of larger clusters. In a mass spectrometric study of high temperature equilibria, Rovner *et al.*²² have taken this into account and have determined heats of atomization of Bi_2 , Bi_3 , and Bi_4 ; these are discussed in relation to our electron affinity measurements. Very recently, Balasubramian and Sumathi²³ performed *ab initio* calculations on group V trimers (P_3 , As_3 , Sb_3 , and Bi_3). The calculations indicate that Bi_3 has a triangular (Jahn–Teller distorted D_{3h}) ground state and calculations are performed on the first four excited states with D_{3h} symmetry. These calculations will be discussed further in comparison to the Bi_3^- photoelectron spectrum.

Bi_4 has been the subject of a number of matrix isolation studies,^{14–16} where optical spectroscopy has probed two excited electronic states. The observed vibrational structure in both optical and Raman spectroscopies provides strong evidence for a tetrahedral structure.

To our knowledge, there have been no reported investigations concerning the negative ions Bi_2^- , Bi_3^- , and Bi_4^- , although there is an unpublished study by Meiwes-Broer and Lutz²⁴ of the ultraviolet photoelectron spectroscopy of Bi_n^- ($n = 2–11$). In the present paper, we report the 351 nm photoelectron spectra of Bi_2^- , Bi_3^- , and Bi_4^- . The most extensive information is obtained from the photoelectron spectrum of Bi_2^- . The anion geometry, vibrational frequency, and dissociation energy are determined. For Bi_2 neutral, electronic states up to 2.1 eV are surveyed, spectroscopic parameters are obtained for three of the low-lying states, and the adiabatic electron affinity is determined. Our results are compared to previous spectroscopic work and to the *ab initio* calculations on Bi_2 and Bi_2^- presented in the accompanying paper.²⁵ The photoelectron spectrum of Bi_3^- probes the electronic structure of Bi_3 , and an adiabatic electron affinity for Bi_3 is determined; however, the determination relies on several assumptions made in the interpretation of the spectrum. For Bi_4^- , a very low signal level precludes extensive analysis. An electron affinity for Bi_4 is estimated from the photodetachment onset.

II. EXPERIMENTAL

The cold cathode discharge metal cluster source^{2(b)} and the photoelectron spectrometer^{26,27} have been described previously in great detail; the important features are summarized here. Ions are formed in a bismuth cold cathode discharge source. The bismuth cathode is an approximately 8 cm long, 10 mm diameter rod (Aesar, 99.9999% purity); a 1/8 in. diam., 2.5 cm deep hole is drilled through the center of the rod to hold the bismuth by friction on a 1/8 in. diameter water cooled stainless steel electrode. The bismuth rod is in electrical contact with the electrode and is floated at -2 to -4 kV with respect to ground. In this manner, a discharge is struck between the cathode and the chamber walls. The primary carrier gas is helium [500 mTorr, flow rate = 4 standard liters per minute (SLPM)], seeded with approxi-

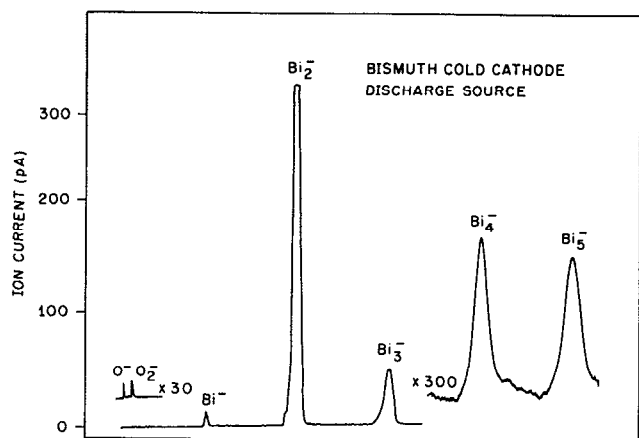


FIG. 1. Mass spectrum from the bismuth cold cathode discharge source.

mately 10% argon to promote cathodic sputtering. The ions formed are allowed to equilibrate with the carrier gas in a 0.25 m long flow tube, at the end of which the negative ions are extracted through a 0.5 mm pinhole into a differentially pumped region. A mass spectrum of the negative ions extracted from the source is shown in Fig. 1. As the mass spectrum shows, Bi_2^- is the dominant ion; optimized currents for each species were 7 pA of Bi^- , 400 pA of Bi_2^- , 45 pA of Bi_3^- , 0.7 pA of Bi_4^- , and 0.7 pA of Bi_5^- measured at a Faraday cup at the end of the beamline.

After extraction, the ion beam is focused, collimated, and accelerated to 680 V for mass selection. Mass selection is performed using a Wien velocity filter ($m/\Delta m \approx 40–50$) and the ion beam is decelerated to 38 V to maximize the ion residence time in the laser interaction region. Laser radiation is provided by an argon ion laser (Spectra-Physics model 2045) operated on a single line (351 nm or 3.531 eV) and using an intracavity etalon to select a single cavity mode. The laser interaction region is enclosed inside an 80 cm optical buildup cavity formed by two highly reflective mirrors ($R_1 = 0.998$, $R_2 = 0.996$) that are within the vacuum system. The optical cavity provides internal build-up powers of 30–60 W from incident powers of 150–200 mW. The servo-loop stabilization scheme for matching the resonant frequencies of the laser cavity and the optical build-up cavity has been explained in considerable detail.²⁶

Electrons are collected perpendicular to the plane formed by the laser and ion beams. Electron energy analysis is accomplished using a hemispherical electrostatic energy analyzer with a resolution of 8–10 meV. The measured energies are corrected with a transformation²⁸ of the electron kinetic energy (eKE) from the laboratory frame of reference to the ion center-of-mass frame. Absolute calibration is provided through measurement of the very accurately known²⁹ O^- electron affinity. In addition, an empirical correction consisting of a linear energy scale compression of approximately 0.5% is used for relative calibration of the data; for this experiment, measurement of the accurately known³⁰ atomic fine structure splittings in the photoelectron spectra of Bi^- and W^- were used to determine the correction. In this manner, absolute electron kinetic energies can be measured to an accuracy of ± 5 meV.

Because the electron collection angle is fixed, the angular dependence of the photodetachment cross section can be studied by rotating the laser polarization with a half-wave plate. The angular dependence of a photodetachment cross section is given by³¹

$$d\sigma/d\Omega = (\sigma_0/4\pi) [1 + (\beta/2)(3 \cos^2\theta - 1)], \quad (1)$$

where θ is the angle between the laser polarization vector and the direction of electron ejection, and β is the asymmetry parameter ($-1 < \beta < 2$). For all of the spectra shown in the figures, the laser polarization is set at the "magic angle" (54.4° , where $3 \cos^2\theta - 1 = 0$) such that the spectral intensities are proportional to the average photodetachment cross section. The relative peak intensities are then independent of the angular distribution, so that they can be used for a Franck–Condon analysis. In order to measure β for each transition, the photoelectron spectra are measured at $\theta = 0^\circ$ and $\theta = 90^\circ$. To determine β accurately for individual peaks, the angular dependence of the largest peaks in the spectra are measured in 10° intervals and the observed intensities are least-squares fit to Eq. (1). These accurately determined values of β can then be used to scale the $\theta = 0^\circ$ and $\theta = 90^\circ$ spectra with respect to one another.

III. RESULTS AND DISCUSSION

A. Bi_2^- photoelectron spectrum

The 351 nm photoelectron spectrum of Bi_2^- is displayed in Fig. 2 and is plotted in terms of electron binding energy ($h\nu - eKE$). At least seven electronic bands are observed, four of which contain resolved vibrational structure. For the bands labeled e and f, it is unclear how many electronic states contribute to the observed structure. We will first discuss the Franck–Condon analysis and assignment of bands a–d. The *ab initio* calculations and previous spectroscopy are then employed in a more speculative assignment and partial analysis of bands e–g. Finally, angular distributions of photoelectrons are presented for most of the bands. The results are compared to angular distribution measurements for atomic Bi^- .

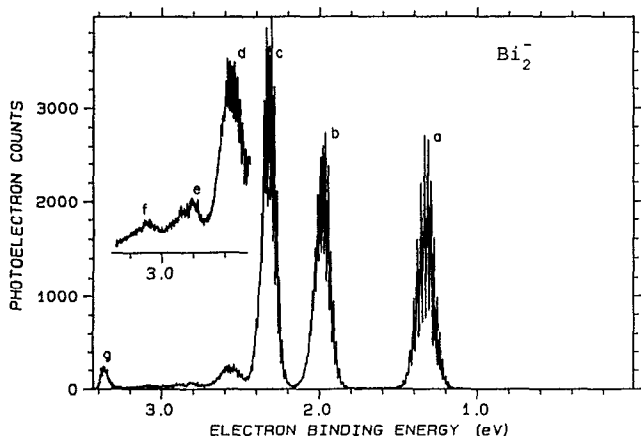


FIG. 2. The 351 nm photoelectron spectrum of Bi_2^- . The inset portion of the spectrum is not a magnification of the data; it was obtained separately with a factor of 15 longer integration time.

In our thermal ion source ($T = 300\text{--}400$ K), only the lowest electronic state (${}^2\Pi_g, 1/2_g$) of Bi_2^- should be populated, as the next lowest energy electronic state (${}^2\Pi_g, 3/2_g$) is calculated²⁵ to lie 8500 cm^{-1} higher. Therefore, all transitions in this spectrum are assumed to arise from the anion ground electronic state. Band a was assigned as a transition to the neutral ground state ${}^1\Sigma_g^+(0_g^+)$, based on the band being the lowest binding energy feature in the spectrum. It will be shown that with such an assignment, the photoelectron spectrum is in general accord with both previous experimental work and *ab initio* calculations.

The Franck–Condon analysis of band a is performed as follows: the anion and neutral ground state potential functions are modeled as Morse oscillators. Franck–Condon factors are computed by numerical integration of the Morse oscillator wave function³² products. The neutral potential constants ($r_e, \omega_e, \omega_e x_e$) are fixed at values determined by high resolution optical spectroscopy,¹¹ while the anion constants are allowed to vary. The line shapes of each vibrational transition are assumed to be Gaussian and the result of the instrumental resolution; because of the small rotational constant (0.023 cm^{-1}) of Bi_2 , the rotational contribution to the line shape is negligible. The parameters allowed to vary in a least-squares fit to the data are the following: the anion Morse potential constants; the electronic origin location; the intensity of the origin transition; the vibrational temperature; and the full width at half-maximum (FWHM) linewidth of the Gaussian instrumental function.

The quality of the fit is strongly dependent on which peak is taken to be the electronic origin and on the direction of the bond length change. For the purpose of assigning the origin, the quality of a given fit could be judged by visual inspection. A large number of origin assignments were attempted; only one choice (shown in Fig. 3) yielded a satisfactory fit, given the accurately known neutral state constants. This choice also yielded a vibrational temperature (320 K) that was consistent with temperatures measured for other ions produced in this source.²

An additional problem lies in determining the direction of the geometry change; a satisfactory fit could only be obtained with a decrease in bond length in going from the anion to neutral. The reason the fit was so sensitive to the direction of the geometry change is the large number of hot bands observed ($\nu'' = 5$) and the relatively long Franck–Condon progression, which enables probing of the anharmonicity of both the anion and neutral potential wells. In our attempts to fit these bands with an incorrect geometry change, we found that the neutral vibrational progression and the hot band progression could not be represented simultaneously by a given simulation. Additional evidence for the anion bond length being larger than that of the neutral is provided from bands b and c. The width of a Franck–Condon profile for an electronic band should reflect the magnitude of the geometry change involved. On inspection, bands b and c appear similar in width to a; however, previous measurements¹⁰ and *ab initio* calculations²⁵ (Table II) show that the bond lengths of the neutral states accessed in b and c are about 0.2 \AA larger than the ground state accessed in band a. For a, b, and c to have similar contours, the anion bond length must

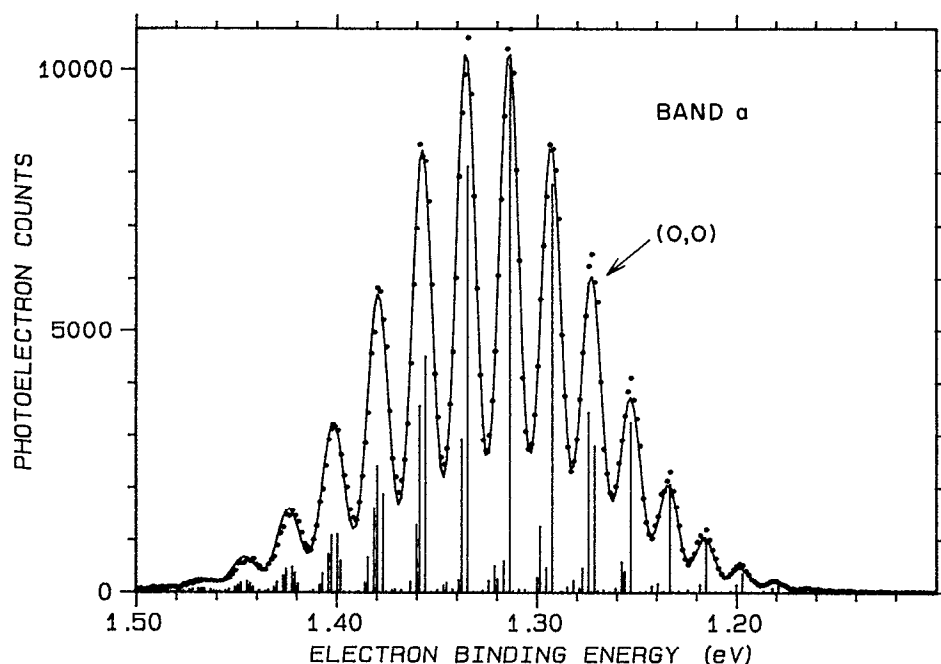


FIG. 3. The Franck-Condon fit of band a [${}^1\Sigma_g^+(0_g^+) \leftarrow {}^2\Pi_g(1/2_g)$]. The dots represent the experimental data, the solid curve is the Franck-Condon simulation, and the vertical sticks represent single vibrational transitions.

lie between those of the ground state and the first two excited states of the neutral, consistent with the direction determined from the ground state fit alone.

The anion constants obtained in the fit are shown in Table I; the calculated spectrum is compared with the actual data in Fig. 3. The uncertainties shown are obtained from varying parameters in the fit and observing changes in χ^2 . The uncertainties listed for the term energies result mainly from calibration inaccuracy. All uncertainties are chosen to correspond approximately to 2σ . The adiabatic electron affinity of Bi_2^- is determined from the electron binding energy of the (0,0) transition to be 1.271(8) eV.

If one tentatively assigns bands b, c, and d based on the

experimentally determined³³ ordering of electronic states in As_2 and with the calculated²⁵ ordering of spin-orbit states, one obtains Bi_2^- electronic state assignments of ${}^3\Sigma_u^+(1_u)$, ${}^3\Sigma_u^+(0_u^-)$, and ${}^3\Delta_u(2_u)$ for bands b, c, and d, respectively. These assignments are justified further in Sec. III B. Franck-Condon fits were performed in the same manner as previously, except the anion Morse potential constants and the anion vibrational temperature were fixed at the values determined in the previous fit. For all three bands, unambiguous electronic origins could be determined. A good fit to the data could not be obtained unless the bond lengths for all three states were constrained to be larger than that of the anion. This result is consistent with both the *ab initio* calcu-

TABLE I. Electronic states accessed in the photoelectron spectrum of Bi_2^- and the molecular constants obtained from a Franck-Condon analysis. Molecular constants that have been fixed for the analysis are also shown.

State	Band ^a	T_0 (cm^{-1})	ω_e (cm^{-1})	$\omega_e x_e$ (cm^{-1})	r_e (\AA)
$\text{Bi}_2^- \quad {}^2\Pi_g(1/2_g)$		-10 250(60)	152(5)	0.53(20)	2.760(10)
$\text{Bi}_2 \quad {}^1\Sigma_g^+(0_g^+)$	a	0	173.06 ^b	2.6596 ^b	2.66 ^b
${}^3\Sigma_u^+(1_u)$	b	5 460(30)	134(5)	0.45(20)	2.863(15)
${}^3\Sigma_u^+(0_u^-)$	c	8 225(40)	132(8)	0.25(15)	2.860(15)
${}^3\Delta_u(2_u)$	d	9 875(50)	125(10)	0.57(30)	2.905(15)
${}^5\Sigma_g^+(0_g^+)$	e	10 826 ^b	106.3 ^b	0.239 ^b	3.022(30)
...	f ^c	$\approx 13\,300$			
...	g ^c	16 850(240)			

^a The bands in Fig. 4 are assigned as transitions from the anion ground state to this state of the neutral.

^b These quantities are fixed at the values determined in Ref. 11.

^c The electronic state assignment is undetermined by our analysis (see the text for possibilities).

TABLE II. A comparison of molecular constants obtained in this work to previous experimental work and to *ab initio* calculations. All constants are in cm^{-1} unless otherwise noted. The best value corresponds to the experimental result that we expect to be most accurate.

State	Constant	This work	Previous experiments	<i>Ab initio</i> ^a	Best value
Bi_2^- $^2\Pi_g (1/2_g)$	T_e^a	- 10 240 (60)		- 5200	- 10240
	ω_e	152 (5)		144	152
	r_e	2.760 (10) Å		2.83 Å	2.760 Å
Bi_2 $X^1\Sigma_g^+ (0_g^+)$	ω_e		173.062 (9) ^{a,d}	151	173.062
	$\omega_e X_e$		0.3758 (10) ^d		0.3758
	r_e		2.6596 Å ^d	2.76 Å	2.6596 Å
$B^3\Sigma_u^+ (1_u)$	T_e	5 480 (30)	5 000 (1000) ^e	6651	5 480
	ω_e	134 (5)	127.05 (10) ^e	114	127.05
	$\omega_e X_e$	0.45 (20)	0.29 (1) ^e		0.29
$A'^3\Sigma_u^+ (0_u^-)$	r_e	2.863 (15) Å	3.00 Å ^e	3.00 Å	2.863 Å
	T_e	8 245 (40)	8 000 (2000) ^e	11780	8 245
	ω_e	132 (8)	141.23 (35) ^e	112	141.23
$^3\Delta_u (2_u)$	$\omega_e X_e$	0.25 (15)	0.37 (4) ^e		0.37
	r_e	2.860 (15) Å	2.85 Å ^e	3.03 Å	2.860 Å
	T_e	9 900 (50)		12833	9 900
$B'^5\Sigma_g^+ (0_g^+)$	ω_e	125 (10)		133	125
	$\omega_e X_e$	0.57 (30)			0.57
	r_e	2.905 (15) Å		2.97 Å	2.905 Å
$A^3\Sigma_u^- (0_u^+)$	T_e		10 826 ^d	13205	10 826
	ω_e		106.3 ^d	91	106.3
	$\omega_e X_e$		0.239 ^d		0.239
$A^3\Sigma_u^- (0_u^+)$	r_e	3.022 (30) Å ^b	3.11 Å ^d	3.24 Å	3.11 Å
	T_e		17 740.7 (1) ^{f,e}	22300	17 740.7
	ω_e		132.403 (15) ^f	140	132.403
$A^3\Sigma_u^- (0_u^+)$	$\omega_e X_e$		0.312 (27) ^f		0.312
	r_e		2.863 Å ^f	2.87 Å	2.863 Å

^a T_e for this work obtained from T_0 and ω_e values in Table I.

^b Error bars on this value do not account for possible modeling errors described in text.

^c Experimental vibrational constants are determined with the inclusion of higher anharmonicities for these states.

^d Effantin *et al.* (Ref. 11).

^e Gerber and Broida [Ref. 10(b)].

^f Erhet and Gerber (Ref. 12).

^g Balasubramanian and Liao (Ref. 25).

lations and the previous experiments shown in Table II. The constants obtained are given in Table I and Fig. 4 illustrates the simulated spectrum obtained for bands b and c. From Fig. 4, it can be seen that the fit to band c does not account entirely for the spectrum at high binding energy. This may be due, in part, to inaccuracies in the Morse representation of the diatomic potential function, as the dissociation asymptote is approached.

The remaining bands (e–g) lack vibrational resolution and cannot be analyzed in the same detail as bands a–d. The lack of vibrational resolution for band g can be explained by the instrumental dropoff in resolution below electron kinetic energies of 0.2 eV. For bands e and f, the lack of vibrational resolution must be due to either small vibrational frequencies ($< 80 \text{ cm}^{-1}$), large Franck–Condon displacements resulting in the piling of numerous sequence bands, overlapping electronic states, or combinations of these.

Band e can be assigned, based on previous experiments.

Effantin *et al.*¹¹ have observed emission to a low-lying 0_g^+ state of Bi_2^- , labeled B' , near $10\,800 \text{ cm}^{-1}$ with the molecular constants listed in Table II. In the photoelectron spectrum, an electronic transition to this state would have an origin at 2.633 eV binding energy. If band e is due to transitions to this state, the lack of vibrational resolution is probably not only due to a small vibrational spacing ($\nu = 106 \text{ cm}^{-1}$), but could be caused by a large Franck–Condon displacement. In order to test whether band e could be assigned to this state, a least-squares fit was performed fixing the anion constants at our previously determined values, and the neutral constants (except r_e) at the values of Effantin *et al.*; only the neutral r_e and the signal intensity were allowed to vary. The result was an r_e of 3.022(30) Å, considerably smaller than the value of 3.11 Å obtained by Effantin *et al.* Our r_e value likely suffers from the breakdown of the Morse oscillator approximation for such a long vibrational progression (ν' up to 25 and within 3500 cm^{-1} of the dissociation asymptote). From the *ab*

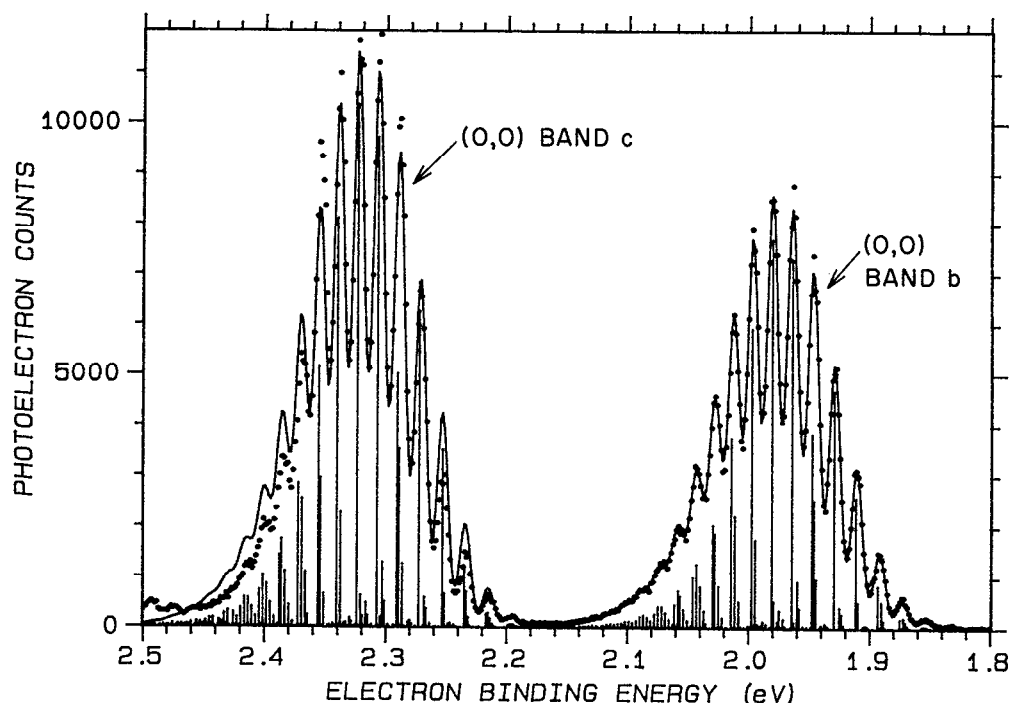


FIG. 4. Franck-Condon fits of bands b [${}^3\Sigma_u^+(1_u) \leftarrow {}^2\Pi_g(1/2_g)$] and c [${}^3\Sigma_u^+(0_u^-) \leftarrow {}^2\Pi_g(1/2_g)$]. It is illustrated in the same manner as Fig. 3.

initio calculations,²⁵ it appears that the most likely candidate for this 0_g^+ state is ${}^5\Sigma_g^+(0_g^+)$ as was previously assigned by Effantin *et al.* In addition, the same calculations show that transitions to the ${}^5\Sigma_g^+(1_g)$ state are likely overlapping transitions to the 0_g^+ state in band e. The possible breakdown of the Morse approximation and the likelihood of an overlapping electronic state suggest that values determined in Franck-Condon fits of band e should not be used quantitatively; however, the simulated contours provide qualitative evidence for the assignment of band e to the B' state.

Bands f and g are considerably more difficult to assign. The contour of band f is very similar to that of the previous band (band e). Use of the band e Franck-Condon contour for band f would place an origin at approximately $13\,300\text{ cm}^{-1}$. For all the bands discussed so far, and the optically observed $A\ {}^3\Sigma_u^-(0_u^+)$ state, the experimentally measured term energies are about 70%–80% of those determined in the *ab initio* calculations.²⁵ Assuming that this will always be the case, the most likely candidates for band f are the ${}^3\Pi_g(0_g^+)$ and ${}^3\Delta_u(3_u)$ states, predicted to lie near $18\,900\text{ cm}^{-1}$. The calculations suggest that these states should have as favorable Franck-Condon factors as bands a–d, but band f is both broad and weak.

Band g appears to be stronger and narrower than bands e and f, although the apparent narrowness may be due to the instrumental dropoff in transmission at low eKE. Because band g falls below 0.2 eV in electron kinetic energy, the resolution, measurement accuracy, and electron collection efficiency are very poor over this band. From the band contour, we place the origin roughly at $3.36(3)\text{ eV}$ binding energy, yielding a term energy of $16\,850(240)$ for the electronic state. This is too low for the state to be the A state observed in optical spectroscopy ($17\,740\text{ cm}^{-1}$), and from the *ab initio*

calculations, the most likely assignment appears to be ${}^3\Pi_g(0_g^-)$. It is unclear why band g is so much stronger than band f, since, according to the calculations, all of the states that can be involved in these transitions should have favorable Franck-Condon factors with the anion ground state. The best explanation we can offer is that the calculated bond lengths for the ${}^3\Pi_g(0_g^+)$ and ${}^3\Delta_u(3_u)$ are an underestimate, relative to the other calculated bond lengths.

The results of angular distribution measurements are summarized in Table III. All of the Bi_2^- transitions for which asymmetry parameters were determined involve transitions from a $(6p\sigma_g)^2(6p\pi_u)^4(6p\pi_g)^1\text{Bi}_2^-$ ground state configuration to either $\sigma_g^2\pi_u^4\pi_g^0$ (${}^1\Sigma_g^+$ ground state) or $\sigma_g^2\pi_u^3\pi_g^1$ (${}^3\Sigma_u^+$ and ${}^3\Delta_u$ excited states) configurations of the neutral, while the most likely assignment of the transition at an eKE of 0.17 eV (band g) is ${}^3\Pi_g(\sigma_g^1\pi_u^4\pi_g^1)$. Therefore, all

TABLE III. Asymmetry parameters for selected Bi_2^- and Bi^- transitions. All transitions are from the anion ground state [${}^2\Pi(1/2_g)$ for Bi_2^- , and 3P_2 for Bi^-] to the specified neutral state. The asymmetry parameters are plotted as a function of eKE in Fig. 5.

Band (Bi_2^-)	Neutral state	eKE (eV)	β
g	Bi_2 , unassigned	0.17	0.00 (10)
d	${}^3\Delta_u(2_u)$	1.035	-0.30 (15)
c	${}^1\Sigma_u^+(0_u^-)$	1.240	-0.10 (10)
b	${}^1\Sigma_u^+(1_u)$	1.583	0.19 (10)
a	${}^1\Sigma_g^+(0_g^+)$	2.260	0.35 (10)
	$\text{Bi}, {}^2D_{3/2}$	0.671	-0.98 (10)
	${}^2D_{3/2}$	1.169	-0.68 (10)
	${}^4S_{3/2}$	2.585	0.42 (10)

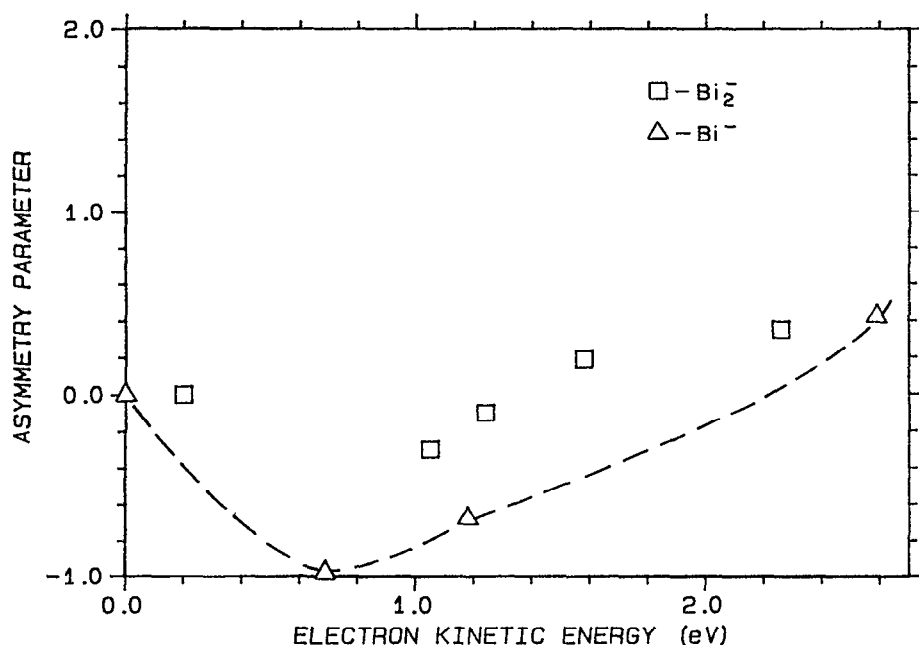


FIG. 5. Asymmetry parameters for selected transitions of Bi^- and Bi_2^- plotted against electron kinetic energy (eKE). The data are given in Table III. The dashed line is a typical curve for detachment of a p electron, which is superimposed on the Bi^- data.

of the detachment orbitals are to first order composed of atomic $6p$ orbitals. To put the angular distribution measurements in perspective, we measured the previously recorded³⁴ Bi^- atomic photoelectron spectrum and obtained angular distributions; the results are also summarized in Table III. All of the transitions in the atomic spectrum are associated with the removal of a $6p$ electron and the assignments are shown in Table III. For atomic p orbital detachment, studied both theoretically and experimentally for O^- ,³⁵ the asymmetry parameter is strongly dependent on electron kinetic energy. Detachment is isotropic at low eKE, favors ejection perpendicular to the laser polarization at intermediate eKE (1–2 V), after which the favoring of parallel ejection increases steadily with increasing eKE.

Figure 5 illustrates the measured asymmetry parameters as a function of eKE. Included in the plot for the atomic measurements is the expected³⁵ $\beta = 0$ for threshold (eKE = 0) detachment of a p electron. As can be seen in Fig. 5, the atomic and molecular asymmetry parameters show similar behavior, although in the molecular case, the angular distributions are more isotropic (β closer to 0). The observed pattern ($\beta = 0$ at low eKE, followed by a drop toward $\beta = -1$, and an increase toward $\beta = 2$ at high eKE) is consistent with detachment of electrons from p -like orbitals. It appears that the atomic parentage of the molecular orbitals plays a role in determining the angular distributions; however, in the molecular case, orientational averaging tends to dampen the angular preferences.

B. The low-lying electronic states of Bi_2

We will now describe all of the gas phase experimental results, including ours, concerning the low-lying electronic states of Bi_2 up to the $A^3\Sigma_u^-(0_u^+)$ state, and compare them to the *ab initio* results from the accompanying paper.²⁵ In 1982, Effantin *et al.*¹¹ reviewed the spectroscopy of the electronic states of Bi_2 . Since that time, the only new results for the low-lying states have been improved constants for the A

state obtained by Ehret and Gerber¹² and the precise determination of the dissociation energy of ground state Bi_2 .¹⁷

Figure 6 summarizes our current knowledge concerning the low-lying electronic states of Bi_2 and the ground state of

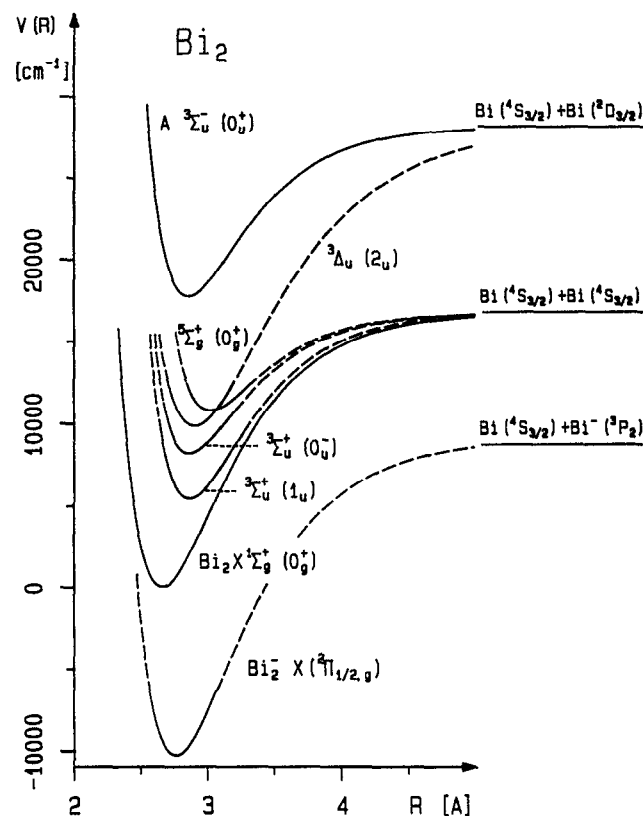


FIG. 6. Potential curves illustrating what is experimentally known about the low-lying electronic states of Bi_2 . Solid curves illustrate portions of the potentials that have been explored experimentally, while the dashed portions of the curves are extrapolations.

Bi_2^- . From this figure and from the photoelectron spectrum, it is evident that the electronic structure of Bi_2 is quite complex. This complexity made *ab initio* calculations extremely important to our assignment of the spectrum. Table II compares the molecular constants obtained in our analysis to previous experiments and to the theoretical results of Balasubramanian and Liao.²⁵

Prior to this work, the only three of these low-lying electronic states that had been assigned completely and linked spectroscopically to the ground state were $X^1\Sigma_g^+$ (0_g^+), $B^5\Sigma_g^+$ (0_g^+), and $A^3\Sigma_u^-$ (0_u^+). The best molecular constants and term energies for these states are listed in Table II.

Table II also presents data obtained by Gerber and Broida¹⁰ (GB) for two electronic states, labeled *B* and *A'*, of Bi_2 . These two states were each observed as a lower state of a single optical transition and vibrational constants were determined through resolution of laser-induced fluorescence (LIF). The vibrational constants determined (ω_e , $\omega_e x_e$) should be fairly accurate (more accurate than those determined by photoelectron spectroscopy), although GB's error bars do not take into account possible vibrational misassignment. The term energies are obtained from temperature dependence studies of the spectra and r_e is obtained simply from the empirical relationship $r_e^2 \omega_e = \text{constant}$. GB assigned both of these states as $\Omega = 0$ states, based on the observation of only a *P* and *R* doublet series in LIF to these states. Our analysis provides assignments for these states.

In this work, we provide molecular constants and term energies for three electronic states—the $^3\Sigma_u^+$ (1_u), $^3\Sigma_u^+$ (0_u^-), and $^3\Delta_u$ (2_u) states. The first excited state of Bi_2 , based on comparison to As_2 (Ref. 33) and on the *ab initio* calculations,²⁵ is expected to be $^3\Sigma_u^+$ (1_u). The relative isolation of this state, both in the calculations and in the spectrum, strongly suggests that the band at 5460 cm^{-1} , labeled *b*, corresponds to this state. The constants obtained for this state are very close to those obtained by GB, for a state which they labeled *B*; however, GB have assigned the state as an $\Omega = 0$ state. It is possible that for the LIF to the 1_u state, only one component of a Λ doublet was accessed by the laser, resulting in the observed absence of a *Q* branch.

Assignment of bands *c* and *d* to either the $^3\Sigma^+$ (0_u^-) or $^3\Delta_u$ (2_u) states is somewhat more problematic. *Ab initio* calculations²⁵ produce energies for these states that are sufficiently close (1650 cm^{-1}), so that the calculations cannot be relied upon entirely for the correct ordering of the states. Our assignment is made on the following basis: The neutral molecular constants obtained from band *c*, particularly the vibrational frequency and term energy, provide a much better match for GB's constants (state labeled *A'*) than do those obtained from band *d*. Therefore, the neutral state of band *c* is assumed to be the same as GB's *A'* state. The dissociation limit of both of GB's states (*B* and *A'*) can be estimated from the simple Morse relationship³⁶ $D_e \approx \omega_e^2 / (4\omega_e x_e)$ to be $19\,370$ and $21\,700\text{ cm}^{-1}$ above the Bi_2 ground state, respectively. These estimates are typically about 20% too high; therefore, it seems likely that both the *B* and *A'* electronic states correspond to the $^4S_{3/2} + ^4S_{3/2}$ asymptote, which lies $16\,778\text{ cm}^{-1}$ above the Bi_2 ground state. This would rule out

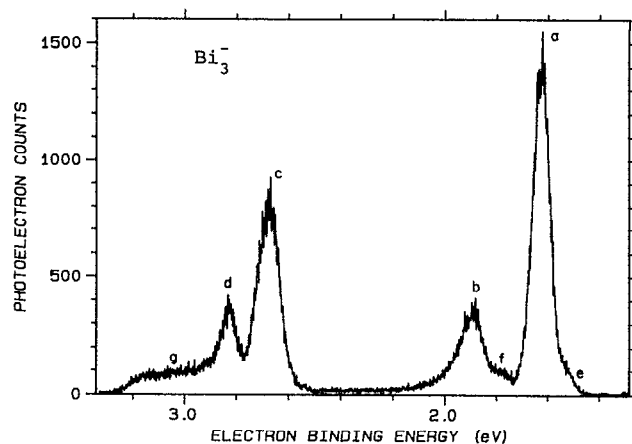


FIG. 7. The 351 nm photoelectron spectrum of Bi_3^- .

assignment of GB's *A'* state and our *c* band to the $^3\Delta_u$ (2_u) state, which corresponds to an $11\,419\text{ cm}^{-1}$ higher asymptote and strongly supports the assignments given in Table I.

To summarize, six of the low-lying (up to the *A* state) electronic states of Bi_2 are now well characterized. Our work has determined molecular constants and provided some new assignments for three of the states.

C. Bi_3^- photoelectron spectrum

The 351 nm photoelectron spectrum of Bi_3^- is shown in Fig. 7. The entire electron kinetic energy range from 0.10 to 3.53 eV was searched; Fig. 7 shows only the region in which photoelectrons were detected. Table IV summarizes the main features of the spectrum.

For both Bi_3 and Bi_3^- , and other group V trimers, the postulated equilibrium structures are either equilateral triangular (Jahn–Teller distorted) or linear. Recently, Balasubramanian and Sumathi²³ have performed calculations on the electronic states of Bi_3 arising from the triangular structure. Complete active space multiconfiguration self-consistent field (CAS-MCSCF) followed by multireference con-

TABLE IV. Features from the Bi_3^- photoelectron spectrum (Fig. 7). Peak center positions and FWHM are obtained from Gaussian fits to features a–d.

Feature	Center electron binding energy (eV)	FWHM (eV)	Assignments and comments
a	1.626	0.079	$^2E' \leftarrow ^3A_2'$
b	1.895	0.112	$^2E' \leftarrow ^3A_2'$
c	2.679	0.103	$^4A_2' \leftarrow ^3A_2'$
d	2.830	0.084	$^4A_2' \leftarrow ^3A_2'$
e			Shoulder on peak a at 1.5 eV binding energy
f			Shoulder on peak b at 1.7–1.8 eV binding energy
g			Broad feature at 2.9–3.2 eV binding energy

figuration interaction (MRCI) calculations revealed a Jahn–Teller distorted 2A_2 ground state and a nearly degenerate (0.04 eV higher in energy) 2B_1 Jahn–Teller distorted first excited state, both of which arise from the ${}^2E'(D_{3h})$ state. Spin–orbit interactions, which are not taken into account at the CAS-MCSCF and MRCI levels, are expected to quench the Jahn–Teller distortion and split the ${}^2E'$ state into D_{3h} double group $E_{5/2}$ and $E_{3/2}$ components. Relativistic configuration interaction (RCI) calculations in the same study suggest a spin–orbit splitting between the two components of approximately 0.3 eV.

The first excited state of Bi_3 is expected to be a ${}^4A_2''$ state, which is calculated to lie 0.87 eV above the ground state at the MRCI level; the authors state that this energy should be increased by 0.2 eV due to spin–orbit mixing with the ground state. For strong spin–orbit coupling,³⁷ the ${}^4A_2''$ state should be split into symmetries resulting from reduction of the direct product of the A_2'' representation and the representation of the quartet spin function, yielding

$$A_2'' \otimes (E_{1/2} \oplus E_{3/2}) = E_{5/2} \oplus E_{3/2}$$

components. Balasubramanian and Sumathi expect the spin–orbit splittings of this and the other excited electronic states of Bi_3 to be between 0.2 and 0.5 eV. Linear electronic states of Bi_3 are also possible; the symmetries of the lowest linear states are expected to be ${}^2\Pi_g$ and ${}^4\Sigma_g^-$, each of which should split into $3/2_g$ and $1/2_g$ components. A calculation of the bending potential for the Bi_3 ground state indicates that the linear ${}^2\Pi_g$ state does not correspond to a minimum on the potential energy surface.

For Bi_3^- , preliminary calculations by Balasubramanian³⁸ suggest that the anion has both an equilateral triangular and a linear electronic state that are nearly degenerate. This is similar to the case for an isovalent anion P_3^- , where the two lowest-lying electronic states are predicted to be a D_{3h} ${}^3A_2'$ state and a ${}^1\Sigma_g^+$ linear state. *Ab initio* calculations on P_3^- by Hamilton and Schaefer³⁹ could not determine conclusively which state is lower.

The photoelectron spectrum in Fig. 7 displays four prominent peaks a–d of comparable linewidth (80–110 meV FWHM). These linewidths are essentially identical to the overall widths of the electronic bands for the most vertical electronic transitions observed in the Bi_2^- spectrum. In addition, the signal level of the strongest peak (a), normalized to laser power and ion current, is about 60%–70% as large as the strongest Bi_2^- transition (c in Fig. 2). The small linewidths and high absolute intensities of these peaks strongly suggest a relatively vertical Franck–Condon transition, i.e., a linear–linear or triangular–triangular transition.

The four peaks can be considered to be two doublets; doublets a and b are split by 0.27 eV and the doublet splitting for c and d is 0.15 eV. The centers of the two doublets are separated by 0.99 eV. Assignment of the upper states of these transitions to the two lowest electronic states of triangular Bi_3 provides good agreement with the calculations²³ for these states, the ${}^2E'$ ground state and ${}^4A_2''$ first excited state. Based on this agreement and the failure of *ab initio* calculations to find a potential energy minimum for the linear ${}^2\Pi_g$

state of Bi_3 , we assign peaks a and b as two components of a neutral–anion ${}^2E' \rightarrow {}^3A_2'$ transition, and peaks c and d as two components of ${}^4A_2'' \rightarrow {}^3A_2'$. The splittings between the two components reflect the neutral state spin–orbit splittings. The anion ${}^3A_2'$ state also has two spin–orbit components A_1' and E'' ; however, at the source temperatures (≈ 320 K), only one component would contain the bulk of the anion population if the splittings were as large as 0.2–0.3 eV.

The four prominent peaks are not the only features observed in the spectrum. Peak a has a broadened shoulder at low binding energy (labeled e) and additional broad structure, labeled f, is detected below peak b. The location of these features is suggestive of hot bands. One possibility is that these features arise from linear Bi_3^- ; however, Franck–Condon factors would be expected to be very small. Another possibility is that an electronically excited spin–orbit level of the anion is populated. The positions of features e and f would place the anion spin–orbit splitting at about 0.1 eV. The most troubling aspect of this possible assignment is the failure to observe analogous hot bands below peak c. The additional width of peak c compared to peak a could easily obscure the feature, however.

The final feature, labeled g, consists of broad structure extending 300 meV above peaks c and d in binding energy, as well as overlapping with peak d. It appears that a large geometry change is involved and the transition could be to a non- D_{3h} state of neutral Bi_3 . For excited states of Bi_3 , Balasubramanian and Sumathi did not depart from the D_{3h} geometry, so it is difficult to predict what additional states are possible at this energy.

Finally, the adiabatic electron affinity of Bi_3 can be estimated. The estimate is dependent both on the correctness of our assignment of peak a and on the ${}^3A_2'$ state of Bi_3^- being the lowest energy state of the anion. The location of the vibrationless origin of transition a is estimated simply by assuming the origin will be shifted from the peak center by the same fraction of the linewidth as in similarly shaped photo-detachment bands (a and b in Fig. 2) in the Bi_2^- spectrum, in which the origin could be assigned rigorously. The result is an adiabatic electron affinity of 1.60(3) eV.

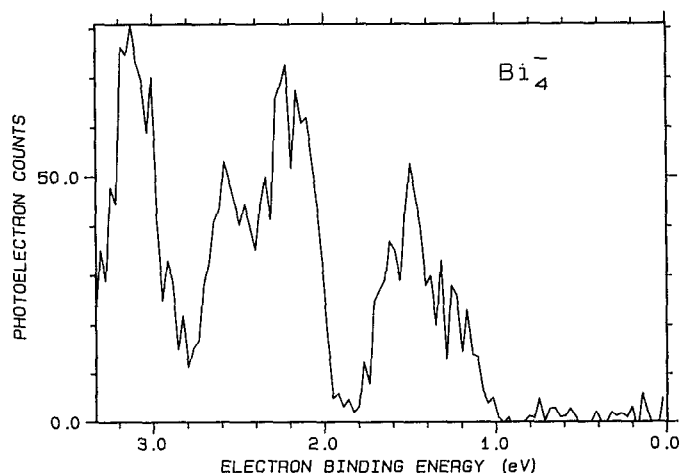


FIG. 8. The 351 nm photoelectron spectrum of Bi_4^- .

D. Bi_4^- photoelectron spectrum

Figure 8 illustrates the photoelectron spectrum of Bi_4^- . The signal level is quite low, making any detailed analysis difficult. The basic features of this spectrum match a more sensitive photoelectron spectrum taken by Meiwes-Broer and Lutz.²⁴ The electron affinity can be approximated from the photodetachment onset to be 1.05(10) eV.

E. Electron affinities and dissociation energies

The observed pattern $\text{E.A.}(\text{Bi}_3) > \text{E.A.}(\text{Bi}_2) > \text{E.A.}(\text{Bi})$ has interesting thermodynamic implications. The dissociation energy difference between Bi_2^- and Bi_2 can be obtained from

$$\begin{aligned} D_0(\text{Bi}_2^-) - D_0(\text{Bi}_2) &= \text{E.A.}(\text{Bi}_2) - \text{E.A.}(\text{Bi}) \\ &= 0.325(13) \text{ eV} [7.49(30) \text{ kcal/mol}], \end{aligned} \quad (2)$$

using $\text{E.A.}(\text{Bi}) = 0.946(10) \text{ eV}$ (Ref. 34) and the Bi_2 electron affinity determined in the present study. Inverting Eq. (2) and using the value $D_e(\text{Bi}_2) = 2.0802(6) \text{ eV}$ (Ref. 17) and a zero point energy correction, we obtain $D_0(\text{Bi}_2^-) = 2.394(12) \text{ eV}$ [55.20(28) kcal/mol]. The negative ion is considerably (7.5 kcal/mol) more bound than the neutral. This result seems surprising because, for Bi_2^- , the additional electron is in an antibonding orbital ($\sigma_g^2 \pi_u^4 \pi_g^1$), the Bi_2^- vibrational frequency is smaller than for the neutral, and the anion bond length is larger than that of the neutral. All of these factors are generally associated with the weakening of a bond; however, we show conclusively that the anion bond is significantly stronger than that of the neutral. To summarize, while the changes in the equilibrium properties of this system (vibrational frequency changes, bond length changes) are well described in the simple MO picture, changes in dissociation energy cannot be similarly explained.

Balasubramanian and Liao's²⁵ calculations show that spin-orbit effects play an important role in stabilizing the anion ground state and this may in part explain the measured dissociation energies; however, they do not calculate an anion dissociation energy. Accounting for the experimentally observed dissociation energy changes provides an interesting challenge to theory.

Much like the dimer anion, the total bond energy of Bi_3^- (energy for dissociation into $\text{Bi}^- + \text{Bi} + \text{Bi}$) is larger than the corresponding total bond energy of Bi_3 (dissociation into $\text{Bi} + \text{Bi} + \text{Bi}$) by the amount

$$\begin{aligned} \text{E.A.}(\text{Bi}_3) - \text{E.A.}(\text{Bi}) &= 0.65(3) \text{ eV} [15.0(7) \text{ kcal/mol}]. \end{aligned}$$

The heat of atomization (ΔH_0°) of Bi_3 has been determined by mass spectrometry to be 85.9(5) kcal/mol (3.72 eV).²² From a simple thermochemical cycle, the heat of atomization of Bi_3^- (into $2\text{Bi} + \text{Bi}^-$) can be determined to be 4.37(4) eV [100.8(9) kcal/mol].

For the $^2E'$ Bi_3 ground state, the occupied molecular orbitals arising from the 6s and 6p atomic orbitals are expected²⁵ to be $1a_1'^2 1e'^4 2a_1'^2 1a_2''^2 2e'^4 1e''^1$. For the $^3A_2'$ state of Bi_3^- ,

the additional electron resides in the e'' orbital. In the linear-combination-of-atomic-orbitals (LCAO) description, this orbital corresponds to an antibonding combination of bismuth p_z orbitals.⁴⁰ The present experiment shows that bond energy increases upon adding an electron to Bi_3 . Therefore, as in the case of Bi_2^- , the measured bond energy changes are contrary to expectations based on simple molecular orbital pictures; one observes an increase in bond energy upon adding an electron to an antibonding orbital.

IV. CONCLUSION

The photoelectron spectra of Bi_2^- , Bi_3^- , and Bi_4^- have been recorded. The Bi_2^- spectrum yields the most extensive information. Spectroscopic parameters were obtained for the anion ground state and three excited states of the neutral. The photoelectron spectrum provided definitive assignments for some states that could not be assigned in previous investigations and greatly improved on what is known about the low-lying electronic states of Bi_2 . *Ab initio* calculations by Balasubramanian and Liao,²⁵ presented in the accompanying paper, were crucial to the assignment process. The adiabatic electron affinity of Bi_2^- was determined to be 1.271(8) eV.

The photoelectron spectrum of Bi_3^- revealed some of the low-lying electronic structure of Bi_3 , which agreed very well with a recent theoretical study by Balasubramanian and Sumathi.²³ The adiabatic electron affinity of Bi_3 was determined to be 1.60(3) eV and depended on certain assumptions that are outlined in the text. The spectrum of Bi_4^- was very weak, making a detailed analysis impractical. The electron affinity was estimated from the photodetachment onset to be 1.05(10) eV.

ACKNOWLEDGMENTS

This work was supported by National Science Foundation Grants No. PHY90-12244 and No. CHE88-19444. The authors thank K. Balasubramanian and D.-W. Liao for a most fruitful collaboration and for furnishing results before publication. We also thank K. H. Meiwes-Broer and H. O. Lutz for providing unpublished results. Finally, G.G. thanks JILA for a Visiting Fellowship.

¹ (a) D. G. Leopold and W. C. Lineberger, *J. Chem. Phys.* **85**, 51 (1986); (b) D. G. Leopold, T. M. Miller, and W. C. Lineberger, *J. Am. Chem. Soc.* **108**, 178 (1986).

² (a) D. G. Leopold, J. Ho, and W. C. Lineberger, *J. Chem. Phys.* **86**, 1715 (1987); (b) K. M. Ervin, J. Ho, and W. C. Lineberger, *ibid.* **89**, 4514 (1988); (c) J. Ho, K. M. Ervin, and W. C. Lineberger, *ibid.* **93**, 6987 (1990).

³ (a) C. L. Pettiette, S. H. Yang, M. J. Craycraft, J. Conceicao, R. T. Laaksonen, O. Cheshnovsky, and R. E. Smalley, *J. Chem. Phys.* **88**, 5377 (1988); (b) G. Ganteför, M. Gausa, K.-H. Meiwes-Broer, and H. O. Lutz, *Faraday Discuss. Chem. Soc.* **86**, 197 (1988); (c) O. Cheshnovsky, K. J. Taylor, J. Conceicao, and R. E. Smalley, *Phys. Rev. Lett.* **64**, 1785 (1990).

⁴ M. D. Morse, in *Advances in Metal and Semiconductor Clusters*, Vol. 1, *Spectroscopy and Dynamics*, edited by M. A. Duncan (in press).

⁵ (a) K. J. Taylor, C. L. Pettiette, M. J. Craycraft, O. Cheshnovsky, and R. E. Smalley, *Chem. Phys. Lett.* **152**, 347 (1988) (Al_3^-); (b) G. Ganteför,

- M. Gausa, K. H. Meiwes-Broer, and H. O. Lutz, *Z. Phys. D* **9**, 253 (1988) (Sn_n^- , Pb_n^-); (c) M. Gausa, G. Ganteför, H. O. Lutz, and K. H. Meiwes-Broer, *Int. J. Mass Spectrom. Ion Proc.* **102**, 227 (1990) (In_n^- , Tl_n^-).
- ⁶J. T. Snodgrass, J. V. Coe, K. M. McHugh, C. B. Friedhoff, and K. H. Bowen, *J. Phys. Chem.* **93**, 1249 (1989) (Se_n^- , Te_n^-).
- ⁷(a) G. M. Almy and F. M. Sparks, *Phys. Rev.* **44**, 365 (1933); (b) G. M. Almy, *J. Phys. Chem.* **41**, 47 (1937).
- ⁸N. Åslund, R. F. Barrow, W. G. Richards, and D. N. Travis, *Ark. Fys.* **30**, 171 (1965).
- ⁹S. P. Reddy and M. K. Ali, *J. Mol. Spectrosc.* **35**, 285 (1970).
- ¹⁰(a) G. Gerber, K. Sakurai, and H. P. Broida, *J. Chem. Phys.* **64**, 3410 (1976); (b) G. Gerber and H. P. Broida *ibid.* **64**, 3423 (1976).
- ¹¹C. Effantin, A. Topouzkhania, J. Figuet, J. d'Incan, R. F. Barrow, and J. Vergès, *J. Phys. B* **15**, 3829 (1982).
- ¹²G. Ehret and G. Gerber, *Opt. Commun.* **51**, 145 (1984).
- ¹³(a) R. A. Teichman III and E. R. Nixon, *J. Chem. Phys.* **67**, 2470 (1977); (b) F. Ahmed and E. R. Nixon, *ibid.* **74**, 2156 (1981).
- ¹⁴(a) V. E. Bondybey and J. H. English, *J. Chem. Phys.* **73**, 42 (1980); (b) V. E. Bondybey, G. P. Schwartz, J. E. Griffiths, and J. H. English, *Chem. Phys. Lett.* **76**, 30 (1980).
- ¹⁵K. Manzel, U. Engelhardt, H. Abe, W. Schulze, and F. W. Froben, *Chem. Phys. Lett.* **77**, 514 (1981).
- ¹⁶(a) B. Eberle, H. Sontag, and R. Weber, *Chem. Phys.* **92**, 417 (1985); (b) *Surf. Sci.* **156**, 751 (1985).
- ¹⁷G. Ehret and G. Gerber, in *Laser Spectroscopy VII*, edited by T. W. Hänsch and Y. R. Shen (Springer, Berlin, 1985).
- ¹⁸L.-S. Wang, Y. T. Lee, D. A. Shirley, K. Balasubramanian, and P. Feng, *J. Chem. Phys.* **93**, 6310 (1990).
- ¹⁹J. Xie and R. N. Zare, *J. Chem. Phys.* **93**, 3033 (1990).
- ²⁰Most recently by M. M. Ross and S. W. McElvany, *J. Chem. Phys.* **89**, 4821 (1988); M. E. Guesic, R. R. Freeman, and M. A. Duncan, *ibid.* **88**, 163 (1988).
- ²¹F. J. Kohl, O. M. Uy, and K. D. Carlson, *J. Chem. Phys.* **47**, 2667 (1967).
- ²²L. Rovner, A. Drowart, and J. Drowart, *Trans. Faraday Soc.* **63**, 2906 (1967).
- ²³K. Balasubramanian and K. Sumathi, *J. Chem. Phys.* (to be published).
- ²⁴K. H. Meiwes-Broer and H. O. Lutz, private communication.
- ²⁵K. Balasubramanian and D.-W. Liao, *J. Chem. Phys.* **95**, 3064 (1991).
- ²⁶K. M. Ervin, J. Ho, and W. C. Lineberger, *J. Chem. Phys.* **91**, 5974 (1989).
- ²⁷D. G. Leopold, K. K. Murray, A. E. Stevens Miller, and W. C. Lineberger, *J. Chem. Phys.* **83**, 4849 (1985).
- ²⁸P. C. Engelking, G. B. Ellison, and W. C. Lineberger, *J. Chem. Phys.* **69**, 1826 (1978).
- ²⁹D. M. Neumark, K. R. Lykke, T. Andersen, and W. C. Lineberger, *Phys. Rev. A* **32**, 1890 (1985).
- ³⁰C. E. Moore, *Atomic Energy Levels* (Nat. Bur. Stand., U. S. GPO, Washington, D.C., 1952), Circ. 467.
- ³¹J. Cooper and R. N. Zare, *J. Chem. Phys.* **48**, 942 (1968).
- ³²K. Cashion, *J. Mol. Spectrosc.* **10**, 182 (1963).
- ³³L. A. Heimbrock, N. Chestnoy, M. Rasanen, G. P. Schwartz, and V. E. Bondybey, *J. Chem. Phys.* **83**, 6091 (1985).
- ³⁴C. S. Feigerle, R. R. Corderman, and W. C. Lineberger, *J. Chem. Phys.* **74**, 1513 (1981).
- ³⁵D. Hanstorp, C. Bengtsson, and D. J. Larson, *Phys. Rev. A* **40**, 670 (1989).
- ³⁶G. Herzberg, *Spectra of Diatomic Molecules* (Van Nostrand-Reinhold, New York, 1950).
- ³⁷G. Herzberg, *Electronic Spectra of Polyatomic Molecules* (Van Nostrand-Reinhold, New York, 1966).
- ³⁸K. Balasubramanian (private communication).
- ³⁹T. P. Hamilton and H. F. Schaefer III, *Chem. Phys. Lett.* **166**, 303 (1990).
- ⁴⁰F. A. Cotton, *Chemical Applications of Group Theory*, 2nd ed. (Wiley-Interscience, New York, 1971), p. 111.